Flame propagation enhancement by plasma excitation of oxygen. Part II: Effects of $O_2(a^1\Delta_g)$

Timothy Ombrello [a,*], Sang Hee Won [a], Yiguang Ju [a], Skip Williams [b,1]

[a] Department of Mechanical and Aerospace Engineering, Engineering Quadrangle, Olden Street, Princeton, NJ 08544, United States
[b] Air Force Research Laboratory, Propulsion Directorate, 1950 Fifth Street, Wright-Patterson AFB, OH 45433, United States

ARTICLE INFO

ABSTRACT

The isolated effect of $O_2(a^1\Delta_g)$ on the propagation of C_2H_4 lifted flames was studied at reduced pressures (3.61 kPa and 6.73 kPa). The $O_2(a^1\Delta_g)$ was produced in a microwave discharge plasma and was isolated from O and O_3 by NO addition to the plasma afterglow in a flow residence time on the order of 1 s. The concentrations of $O_2(a^1\Delta_g)$ and O_3 were measured quantitatively through absorption by sensitive off-axis integrated-cavity-output spectroscopy and one-pass line-of-sight absorption, respectively. Under these conditions, it was found that $O_2(a^1\Delta_g)$ enhanced the propagation speed of C_2H_4 lifted flames. Comparison with the results of enhancement by O_3 found in part I of this investigation provided an estimation of 2–3% of flame speed enhancement for 5500 ppm $O_2(a^1\Delta_g)$ addition from the plasma. Numerical simulation results using the current kinetic model of $O_2(a^1\Delta_g)$ over-predicts the flame propagation enhancement found in the experiments. However, the inclusion of collisional quenching rate estimations of $O_2(a^1\Delta_g)$ by C_2H_4 mitigated the over-prediction. The present isolated experimental results of the enhancement of a hydrocarbon fueled flame by $O_2(a^1\Delta_g)$, along with kinetic modeling results suggest that further studies of $C_nH_m + O_2(a^1\Delta_g)$ collisional and reactive quenching are required in order to correctly predict combustion enhancement by $O_2(a^1\Delta_g)$. The present experimental results will have a direct impact on the development of elementary reaction rates with $O_2(a^1\Delta_g)$ at flame conditions to establish detailed plasma–flame kinetic mechanisms.

© 2010 The Combustion Institute. Published by Elsevier Inc. All rights reserved.

1. Introduction

The development of residence time restricted systems, such as high-speed air-breathing propulsion vehicles, has created the challenges of achieving efficient and reliable ignition, flame propagation, and flame stabilization. Supersonic combustion, for example, constrains the flow residence time to millisecond time scales in the combustor, therefore limiting the time for chemical reaction. In this case the flow residence time is comparable to the chemical reaction time and becomes a more significant problem when using hydrocarbon based fuels instead of hydrogen because of slower initiation times. Therefore, the development of new methods to decrease ignition delay times and increase flame stabilization and flame propagation rates are critical for the development of vehicles capable of hypersonic flight.

There are two methodologies to overcome the characteristic time mismatch, namely increasing the flow residence time or decreasing the chemical reaction time. Modifying the flow times through geometric changes are effective, but can create significant thermal management difficulties and pressure losses. Therefore, applying new techniques to increase the rate of fuel oxidation and overall chemical kinetics has attracted much attention.

One of the potential solutions to increase the rate of combustion and chemical reactions is the application of plasma activation. Plasma-assisted combustion produces elevated temperatures, radicals, excited species, ions, and electrons that have the possibility to increase the rate of fuel oxidation. Because of the significant promise of plasma, much research has been performed using a variety of plasma discharge systems including plasma torches/jets [1–4], gliding arc discharges [5–7], fast ionization waves [8,9], and nanosecond repetitively pulsed discharges [10,11], as well as through electric field interactions [12–14], microwave discharges [15–17], and many others. The investigations have shown definitively that plasma can enhance combustion processes with decreased ignition times and lower ignition temperatures [6,7,10,11,19,20], increased flame propagation [13,14,16–18], and

* Corresponding author. Present address: Air Force Research Laboratory, Propulsion Directorate, 1950 Fifth Street, Building 18 D, Room D229, Wright-Patterson AFB, OH 45433, United States. Fax: +1 937 656 4659.
E-mail addresses: timothy.ombrello@wpafb.af.mil (T. Ombrello), sangwon@princeton.edu (S.H. Won), yju@princeton.edu (Y. Ju), skip.williams@maui.afmc.af.mil (S. Williams).
1 Present address: Air Force Research Laboratory, Directed Energy Directorate, Detachment 15, 535 Lipoa Parkway, Suite 200, Kihei, Maui, Hawaii 96753, United States.

			Form Approved OMB No. 0704-0188

Report Documentation Page

1. REPORT DATE **10 MAR 2010**	2. REPORT TYPE	3. DATES COVERED **00-00-2010 to 00-00-2010**

4. TITLE AND SUBTITLE **Flame propagation enhancement by plasma excitation of oxygen. Part II: Effects of O2(a1Dg)**	5a. CONTRACT NUMBER
	5b. GRANT NUMBER
	5c. PROGRAM ELEMENT NUMBER
6. AUTHOR(S)	5d. PROJECT NUMBER
	5e. TASK NUMBER
	5f. WORK UNIT NUMBER

7. PERFORMING ORGANIZATION NAME(S) AND ADDRESS(ES) **Princeton University,Department of Mechanical and Aerospace Engineering,Princeton,NJ,08544**	8. PERFORMING ORGANIZATION REPORT NUMBER

9. SPONSORING/MONITORING AGENCY NAME(S) AND ADDRESS(ES)	10. SPONSOR/MONITOR'S ACRONYM(S)
	11. SPONSOR/MONITOR'S REPORT NUMBER(S)

12. DISTRIBUTION/AVAILABILITY STATEMENT
Approved for public release; distribution unlimited

13. SUPPLEMENTARY NOTES

14. ABSTRACT
The isolated effect of O2(a1Dg) on the propagation of C2H4 lifted flames was studied at reduced pressures (3.61 kPa and 6.73 kPa). The O2(a1Dg) was produced in a microwave discharge plasma and was isolated from O and O3 by NO addition to the plasma afterglow in a flow residence time on the order of 1 s. The concentrations of O2(a1Dg) and O3 were measured quantitatively through absorption by sensitive off-axis integrated-cavity-output spectroscopy and one-pass line-of-sight absorption, respectively. Under these conditions, it was found that O2(a1Dg) enhanced the propagation speed of C2H4 lifted flames. Comparison with the results of enhancement by O3 found in part I of this investigation provided an estimation of 2?3% of flame speed enhancement for 5500 ppm of O2(a1Dg) addition from the plasma. Numerical simulation results using the current kinetic model of O2(a1Dg) over-predicts the flame propagation enhancement found in the experiments. However, the inclusion of collisional quenching rate estimations of O2(a1Dg) by C2H4 mitigated the over-prediction. The present isolated experimental results of the enhancement of a hydrocarbon fueled flame by O2(a1Dg), along with kinetic modeling results suggest that further studies of CnHm + O2(a1Dg) collisional and reactive quenching are required in order to correctly predict combustion enhancement by O2(a1Dg). The present experimental results will have a direct impact on the development of elementary reaction rates with O2(a1Dg) at flame conditions to establish detailed plasma?flame kinetic mechanisms.

15. SUBJECT TERMS

16. SECURITY CLASSIFICATION OF:			17. LIMITATION OF ABSTRACT	18. NUMBER OF PAGES	19a. NAME OF RESPONSIBLE PERSON
a. REPORT **unclassified**	b. ABSTRACT **unclassified**	c. THIS PAGE **unclassified**	**Same as Report (SAR)**	**13**	

enhanced flame stabilization [2,3,7,15]. It has been stated in a recent review of plasma-assisted combustion that "artificial initiation of chemical chains by low temperature plasma of gas discharges does exist," but there is a lack of data from controlled and well-defined experiments [21]. Experiments that explore the enhancement of combustion processes with plasma are plagued with highly coupled thermal and kinetic interactions, making it difficult to isolate the key species and the various enhancement mechanisms.

Therefore, one of the major challenges associated with understanding the plasma–flame interaction is the isolation of the effect of individual species and obtaining a fundamental knowledge of specific enhancement processes. Plasma discharges can produce an incredibly wide range of stable and metastable species that have the potential to enhance combustion, especially when the discharge is in a premixture of fuel and oxidizer. A practical system will require an understanding of each and every one of the species and their interaction in a combustion process. The inclusion of each and every species and their associated reactions would render kinetic mechanisms nearly impossible to use. More importantly, there is a lack of understanding of what species and reaction pathways are the most important. Realistically, there will only be a few species that are critical to the enhancement mechanism. Therefore, careful selection of the plasma-produced species is warranted in order to make the largest impact on achieving an understanding of the plasma–flame interaction and developing kinetic models for accurate predictive capabilities.

Experiments need to be performed to isolate the individual effects that may be present in plasma–combustion systems and determine to what extent they participate in the enhancement processes. Isolating the individual enhancement mechanisms can be difficult because plasma–combustion systems can be highly coupled with complex hydrodynamics, species diffusion, and thermal processes. The coupled processes do not allow the underlying physics and chemistry involved to be identified clearly. Furthermore, there exists the additional complication of plasma-produced species lifetimes when trying to observe individual enhancement pathways.

Shown in Fig. 1 is an illustration of some of the common plasma-produced species and their lifetimes as a function of pressure. Depending upon the application and the species of interest, decoupling the plasma–flame interaction can be challenging. For example, when the pressure is sufficiently low (sub-atmospheric), plasma-produced species have long lifetimes and the potential to be transported significant distances. On the other hand, at extremely high pressures, plasma-produced species have a very short lifetime because of high rates of recombination and collisional quenching. Since the concentration of species is proportional to the pressure and hence number density, the lower the pressure, the longer the mean free path and the smaller the collision frequency. To minimize the loss of radicals and excited species, the pressures need to be low or the plasma has to be located almost directly in contact with the reaction zone to enhance combustion. Unfortunately, decoupling of the plasma–combustion interaction
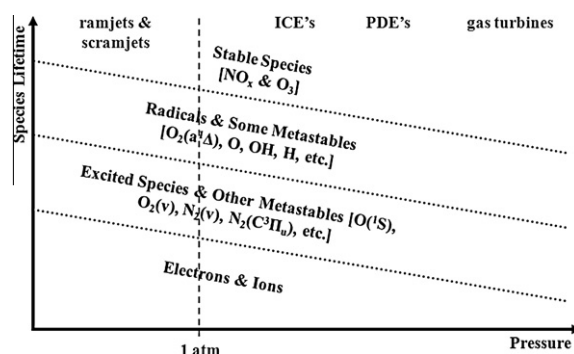

Fig. 1. Lifetimes of plasma-produced species as a function of pressure in relation to common systems applications.

becomes increasingly difficult as the plasma is moved closer to the reaction zone. Some of the major problems that arise are electric field and flow disturbance effects. These complications make it difficult to elucidate the fundamental interaction, especially when trying to understand the effects of specific plasma-produced species.

Furthermore, plasma can couple energy into combustion systems via many different pathways producing a diverse range and significant number of species including radicals, excited species, ions, and electrons. As a starting point, plasma-produced species such as NO_x and O_3 are very important, have been studied in detail, and are integrated with combustion kinetics [5,6]. Reactive radicals such as O, OH, and H have been studied to a lesser extent in plasma-assisted combustion systems [19,22], but are fully integrated with traditional combustion chemistry. Therefore, one of the key links between combustion and plasma chemistry that remain are with ions, electrons, and excited species. Among ions, electrons and excited species, there has been some work on their effects in combustion systems, but the governing kinetics are weakly understood [23–25]. The hope is that the inclusion of ions, electrons, and excited species will open up the possibility of new and faster reaction pathways that can enhance critical combustion phenomena significantly with a high degree of chemical selectivity. One of the species that has attracted much attention is $O_2(a^1\Delta_g)$, also known as singlet delta oxygen. It has a low excitation energy of 0.98 eV and therefore is produced in almost all oxygen containing plasmas. Singlet delta oxygen also has a higher oxidation potential than O_2 and has significantly long radiative lifetime (> 4000 s) because of a spin forbidden transition to the ground state [26].

There have been numerous computational studies aimed to quantify the enhancement of ignition and flame stabilization by $O_2(a^1\Delta_g)$. Starik and Titova showed that when O_2 was excited to its first electronic state of $O_2(a^1\Delta_g)$ by laser radiation in a supersonic flow of H_2-air, the induction time and temperatures necessary for ignition behind a shockwave were reduced significantly [27]. They attributed the enhancement to come from new pathways with $O_2(a^1\Delta_g)$ to generate active species, such as O, H, and

OH. Work was also performed computationally using an electrical discharge to achieve similar results as the laser radiation [28]. Detailed investigations of the ignition kinetics with the presence of $O_2(a^1\Delta_g)$ by non-equilibrium excitation in a H_2–O_2 system was reviewed in a paper by Popov [29]. The review pointed out that if the quenching of $O_2(a^1\Delta_g)$ by H_2 is not considered, there will be a gross overestimate of the amount of enhancement because the collisional quenching rate increases significantly with temperature. Popov also emphasized was that there is a lack of experimental studies of the effect of electronically excited species on combustion phenomena.

Starik, Kuleshov, and Titova studied ignition enhancement in an H_2–O_2 mixture. Here, they created $O_2(a^1\Delta_g)$ along with $O(^1D)$ with a flash photolysis approach: O_3 was the sensitizer species and the radiation was from a UV laser beam. The collective effect of these two species led to decreased ignition delay times by several orders of magnitude [30]. The absorbed energy by UV laser radiation was very small compared to the energy required for the same amount of enhancement by thermal means, indicating the distinct advantage of having strong non-equilibrium excitation for combustion enhancement. Nevertheless, the results were not verified with experiments.

Kozlov, Starik, and Titova conducted numerical simulations to show the enhancement of H_2–O_2 flame speed with $O_2(a^1\Delta_g)$ addition [31]. The results showed that a concentration of 10% $O_2(a^1\Delta_g)$ gave more than a 50% increase in the laminar flame velocity. Lean mixtures were enhanced more than stoichiometric and rich mixtures because of the chain initiation and branching reactions involved. Bourig et al. extended the numerical modeling by investigating ignition and flame propagation, as well as flame stabilization by $O_2(a^1\Delta_g)$ [32].

Experimental validation of the enhancement of $O_2(a^1\Delta_g)$ on ignition was introduced by measurement of the emission from OH^* at 306.4 nm [33]. Here they monitored OH^* behind a shock-wave in an H_2–O_2 mixture that was subjected to an electrical discharge. It was found that there was accurate reproduction of the experimental results with the kinetic mechanism and that OH^* might be a good indicator for enhancement by $O_2(a^1\Delta_g)$ because of the elevated radical pool concentrations. Skrebkov and Karkach performed subsequent simulations using the ignition and emission spectroscopy results from Ref. [33] and showed that there was reasonable agreement; however, they emphasized that the main stumbling block was the "availability of experimentally evaluated amounts of $O_2(a^1\Delta_g)$," as well as other plasma excited species [34].

There has only been one experimental investigation of the effects of $O_2(a^1\Delta_g)$ on combustion phenomena. Smirnov et al. performed experiments aimed at isolating the effect of $O_2(a^1\Delta_g)$ on the ignition of H_2–O_2 mixtures at low pressure between 1.33 kPa and 2.67 kPa [35]. The results showed decreased induction times. Here, they noted that to achieve the same delay by heating the mixture, the energy input would be 4.4 times greater than that needed to produce $O_2(a^1\Delta_g)$. The experiments were designed to minimize all other plasma-produced species, especially O and O_3, with the injection of Hg and its oxide (HgO) into the flow. The results showed that there was a 100-fold decrease in the emission from O, but no absolute measurement of its concentration was performed. Furthermore, the O_3 was not measured and the $O_2(a^1\Delta_g)$ was only measured through emission. Therefore, the measurements did not provide quantitative concentrations of all the major species of enhancement in the system. Even though the experiments were the first of their kind in an attempt to isolate the effect of $O_2(a^1\Delta_g)$ and the results agreed reasonably well with their previous calculations [36,37] it was not certain whether $O_2(a^1\Delta_g)$ was the only species causing the enhancement. In addition, the experiments were conducted only for an H_2–O_2 mixture.

Therefore, there is scarce experimental data detailing and quantifying the effect of electronically excited species, specifically $O_2(a^1\Delta_g)$, on combustion phenomena. A majority of the numerical and experimental work has been focused on the H_2–O_2 reaction system, with no experimental studies of the isolated effects of $O_2(a^1\Delta_g)$ on hydrocarbon based fuels. There have been no experimental studies at higher pressures, greater than 2.67 kPa, where a structured flame can exist. Furthermore, there have been no experimental studies with quantitative concentration measurements of $O_2(a^1\Delta_g)$, O, and O_3.

The goal of the present work was to isolate and measure quantitatively the effects of $O_2(a^1\Delta_g)$ on the enhancement of flame propagation using a hydrocarbon based fuel, as well as to understand the kinetic mechanisms involved. The enhancement of flame propagation speeds were investigated through the development of an integrated plasma–combustion experimental platform where $O_2(a^1\Delta_g)$ was produced, transported, and absolute measurements taken through integrated-cavity-output absorption spectroscopy. A low power microwave coupled plasma was used to activate Ar/O_2 as the oxidizer co-flow of low pressure C_2H_4 lifted flames. The individual effects of $O_2(a^1\Delta_g)$ were isolated by NO addition to catalytically remove O_3 and O, the two major quenching species of $O_2(a^1\Delta_g)$. The experiments provide the first experimental evidence of the isolated effect of $O_2(a^1\Delta_g)$ on the propagation of a hydrocarbon fuel based flame. The results will provide important steps towards developing a comprehensive predictive model for plasma–combustion systems with detailed and well-defined experimental results.

2. Experimental system

The experimental platform was designed to have two separate apparatuses consisting of a lifted flame burner and a plasma-produced species diagnostics system. The two apparatuses shared the same flow controllers, plasma device, and inert wall surfaces. A schematic of the experimental platform is shown in Fig. 2.

2.1. Plasma-assisted lifted flame system

A laminar lifted flame burner was adopted for the combustion platform and was placed in a variable pressure chamber that could be used from atmospheric pressure down to 2.67 kPa with the installed vacuum and flow system. The lifted flame burner consisted of a central fuel jet with a diameter of 1.04 mm and was located in a 90 mm inner diameter fused silica (quartz) tube to contain the co-flow of O_2 and Ar in the chamber. The fuel nozzle was aerodynamically shaped to produce a uniform velocity profile at the exit. To ensure that the co-flow was uniform, two stainless steel meshes coated with quartz for chemical inertness were separated by 3 cm and were located between the oxidizer inlet of the burner and the fuel jet exit. The gases used in the experiments were C_2H_4 for the fuel and ultra-high purity O_2 (99.99%) and Ar (99.95%) mixed for the oxidizer. The flow rate of the fuel was controlled with a calibrated mass flow meter while the O_2 and Ar were controlled with calibrated sonic nozzles to give flow rate uncertainties of less than 1%.

To excite the co-flow in the low pressure experiments, an electrodeless microwave discharge (McCarroll cavity driven by an Opthos MPG-4M microwave power supply) with up to 100 W of power was used external to the chamber, upstream of the lifted flame burner to activate the O_2 in the mainly Ar flow (15% O_2 in 85% Ar for 3.61 kPa and 11.9% O_2 in 88.1% Ar for 6.73 kPa). The plasma was initiated in the microwave cavity by seeding the upstream flow with ionized gas created by a high-voltage, high-frequency Tesla coil. The mixture of ultra-high purity O_2/Ar was
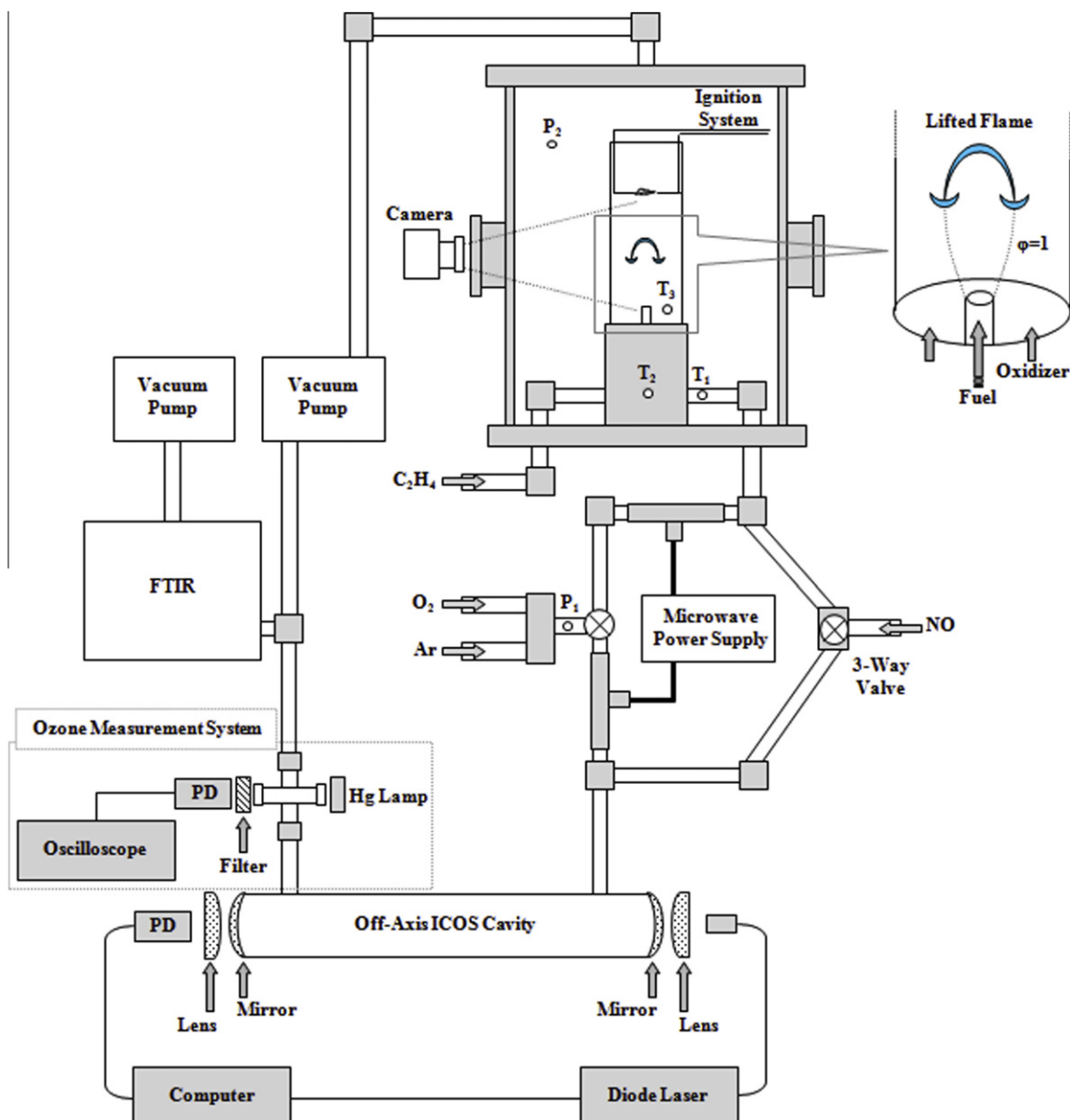
Fig. 2. Experimental set-up schematic of variable pressure lifted flame burner integrated with microwave plasma discharge device and plasma flow diagnostics system. The abbreviation "PD" denotes photodetector.

therefore activated by the self-sustained microwave discharge which was maintained when the Tesla coil was switched off. The plasma system was chosen because of its flexibility of being used external to a quartz tube flow system, as well as its ease of tuning and stability for the range of pressure used in the experiments. Furthermore, the lower power output of the plasma system produced a glow discharge with lower reduced electric field and an electron energy distribution function that was peaked at lower electron temperature where significant concentrations of $O_2(a^1\Delta_g)$ could be excited from ground state O_2. Nevertheless, the microwave discharge produced excited Ar, as well as multiple oxygen containing species including O, O_3, $O_2(v)$, $O(^1D)$, $O(^1S)$, $O_2(a^1\Delta_g)$, $O_2(b^1\Sigma_g)$, etc.

The high velocity fuel jet (approximately 20–40 m/s) and low velocity co-flow (approximately 0.15–0.2 m/s) created a mixing layer with a stoichiometric contour where the premixed flame head of a lifted flame was located (shown in the top right inset in Fig. 2). The lifted flame, which is also called a tribrachial (triple) flame, had a premixed flame head and diffusion flame tail where the flame was always anchored on the stoichiometric contour.

The lifted flame could be located at different distances from the fuel jet nozzle depending upon the local flow velocity. For a fixed flow field, the flame is located in a stationary position where the lifted flame speed at the premixed flame head is balanced with the local flow velocity. In Fig. 3, photographs are shown of stationary C_2H_4 lifted flames as a function of fuel jet velocity for a pressure
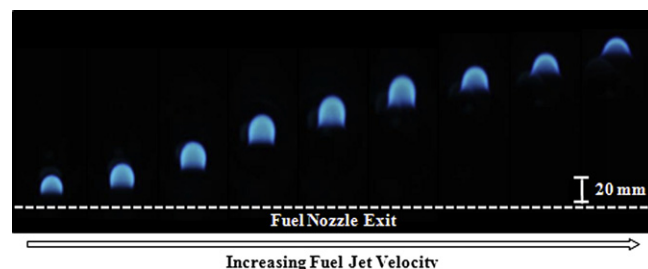

Fig. 3. Photographs of C_2H_4 lifted flames at stationary positions for different fuel jet velocities at 6.73 kPa.

of 6.73 kPa. If the flame speed increases, the liftoff height decreases to re-establish a local dynamic balance between the flame speed and flow velocity.

Due to the slow laminar boundary layer development and the velocity and concentration gradients created, the lifted flame height is very sensitive to the changes in flame speed and therefore provides excellent flame geometry for the direct observation of flame speed enhancement. Since the fuel and oxidizer are not mixed far upstream of the flame, there is very short residence time for the fuel and oxidizer to react in the cold flow. The short residence time helps to further decouple the enhancement effects to be directly from reactions in the flame zone and not far upstream in the cold un-reacted flow.

All surfaces that the plasma afterglow gases came in contact with were treated to be chemically inert. The tubing used was fused silica (quartz), the fittings were 316 stainless steel (non-magnetic) and the lifted flame burner was coated with silica (Restek Silcosteel). The inert surfaces mitigated the quenching from active wall surfaces and promoted the transport of $O_2(a^1\Delta_g)$ to the flame. Multiple temperatures and pressures were monitored and recorded in the system with thermocouples and pressure transducers, respectively. Temperatures were measured at points T_1, T_2, and T_3 shown in Fig. 2 corresponding to the burner inlet tube surface temperature, burner surface temperature, and co-flow gas temperature, respectively. Additionally, the pressure upstream of the microwave plasma and in the chamber respectively at points P_1 and P_2 in Fig. 2 were continuously monitored and recorded.

2.2. Plasma afterglow diagnostics systems

The plasma activated oxidizer flow was run through a series of diagnostics to quantify the concentrations of species produced by the plasma. The flow system used the same chemically inert flow surfaces and residence times for a direct comparison to the lifted flame system. The diagnostics were not run in situ with the flame system, but instead as two separate systems with common flow control and plasma discharge. The systems were used separately because having the ICOS cavity between the plasma and flame would double the transport residence time and decrease the concentrations of the species of interest. For the 3.61 kPa and 6.73 kPa experiments, the residence time from the plasma to the end of the ICOS cavity was approximately 1320 ms and 1680 ms, respectively and between the plasma and flame in the burner were approximately 910 ms and 1470 ms, respectively.

2.2.1. Quantitative $O_2(a^1\Delta_g)$ Measurement Using Off-Axis ICOS

The $O_2(a^1\Delta_g)$ produced by the microwave plasma discharge was measured by using highly sensitive integrated-cavity-output spectroscopy by absorption at the (1, 0) band of the $b^1\Sigma_g^+ - a^1\Delta_g$ Noxon system [38]. The ICOS system measured the average number density of $O_2(a^1\Delta_g)$ across an 82.5 cm long (approximately 1500 ms residence time) absorption cell downstream of the plasma. The effective path length was greater than 78 km due to multiple passes and provided accurate measurements down to 10^{14} molecules/cm³. In Fig. 4 the transmittance spectrums from the ICOS cavity for the experimental conditions with and without NO addition and plasma activation are shown. The absorption feature demarcated by the red box shows the location of the Q(12) transition of $O_2(a^1\Delta_g)$, which was the primary transition of interest [38]. The Q(12) transition was chosen for absorption measurements because there was no interference between it and any of the absorption features of other species present in the flow. In Fig. 5, the measured absorption profile of $O_2(a^1\Delta_g)$ using the Q(12) transition for plasma-activated Ar/O_2 at 3.61 kPa is shown. The fitted curve in Fig. 5 was a function of the absorption path-length and cross-section, as well as broadening from pressure
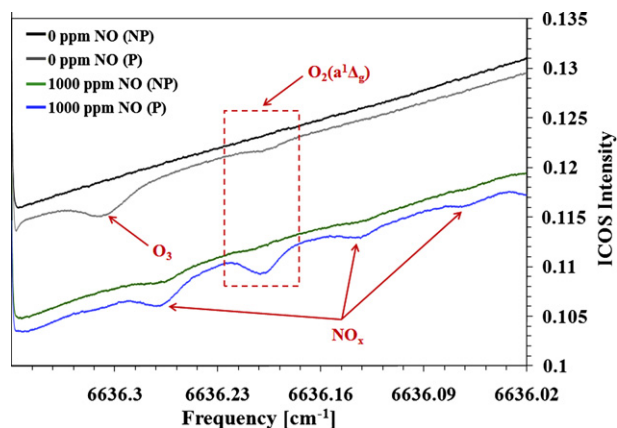

Fig. 4. ICOS transmittance spectrum with and without NO addition and plasma activation (P and NP are plasma and no plasma, respectively).
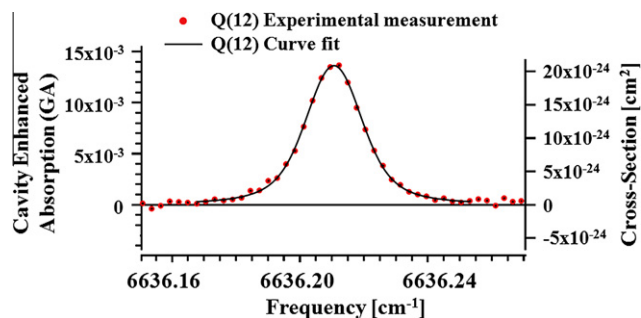

Fig. 5. Cavity-enhanced absorption (GA) measurement of $O_2(a^1\Delta_g)$ obtained by tuning the laser over the Q(12) transition.

and temperature. A more detailed description of the measurement and curve fitting process to obtain absolute number densities of $O_2(a^1\Delta_g)$ can be found in previous work [38].

2.2.2. Quantitative absorption measurements of O_3

The production of $O_2(a^1\Delta_g)$ also resulted in significant production of O_3, and therefore it had to be measured quantitatively. To accomplish this, a one-pass, line-of-sight absorption cell was adopted. The absorption cell was comprised of a stainless steel compression cross fitting with the side arms made of quartz tubes capped with UV quality windows. At one window, a mercury light with stable output provided ultraviolet light at the wavelengths covering the Hartley band of O_3. A 10 nm notch filter isolating only the 253.7 nm mercury line was placed at the exit of the absorption cell, followed by a photodiode detector. The wavelength of 253.7 nm was used because O_3 has a peak absorption cross-section there of 1.137×10^{-17} cm² (at 300 K) [39]. No other species present in the flow absorb at this wavelength. Therefore, the change in the transmittance of the cell with the plasma on and off could be used to determine the O_3 concentration through the Beer–Lambert law

$$N_{\text{ozone}} = \frac{-\ln\left(\frac{I}{I_0}\right)}{\sigma_{\text{ozone}} L} \tag{1}$$

where N_{ozone} is the absolute number density of the absorbing species, O_3, I the intensity of light with the presence of O_3, I_0 the intensity of light without the presence of O_3, σ_{ozone} the absorption cross-section of O_3 at the excitation wavelength (253.7 nm), and L the path length in the absorption cell (12.48 cm). The concentration was then calculated in parts per million (ppm) of O_3 with an uncertainty

of approximately ±2% and a minimum detectable threshold of approximately 15 ppm. The uncertainty and minimum detectable threshold came from the fluctuations in the intensity of the mercury light as a function of time during the experiments.

2.2.3. FTIR spectroscopy for NO and NO_2 measurement

The isolation of $O_2(a^1\Delta_g)$ in the plasma afterglow was achieved with the addition of a small concentration of NO to the flow. The details of this approach are described in Section 2.3. Therefore, quantitative measurements of NO and NO_2 were required to confirm the presence of these species in the system. To accomplish these measurements the flow was split downstream of the O_3 absorption cell to allow sampling with Fourier Transform Infrared (FTIR) spectroscopy (Fig. 2). The pressure and temperature were fixed at 2 kPa and 373 K, respectively, in the FTIR cell for all experimental measurements to maintain sufficient flow rates and sampling times. The absorption features of NO and NO_2 were chosen where there would be no chance of interference from changes in the background or other species.

2.3. Isolation of $O_2(a^1\Delta_g)$ and O_3 from other plasma-produced species

To avoid the complications of plasma disturbances in the combustion system, the flow was activated far upstream of the lifted flame. With the flow rates used in the experiments, the average residence times between the plasma and the flame was approximately 1 s. The significantly long residence time was chosen in order to quench the plasma-produced species that were not of interest in the experiments. Furthermore, since the focus of the current experiments were to isolate $O_2(a^1\Delta_g)$, Ar was used as the inert instead of N_2. Using Ar served two purposes. First, Ar has only electronic excitation requiring 11.6 eV for the first electronic level. Therefore, when using the low power microwave system, most of the energy will then be deposited into the O_2 to produce O, O_3, $O_2(a^1\Delta_g)$, $O_2(b^1\Sigma_g)$, and metastable O and Ar. Second, without N_2, there would be no nitrogen containing species produced, specifically NO or NO_2, simplifying the chemistry in the plasma and in the post-plasma flow.

With the 1 s residence time, the only two species that have long enough lifetime to allow for measurement and introduction to a combustion system are O_3 and $O_2(a^1\Delta_g)$. A list of the primary quenching reactions of the oxygen containing species is given in Table 1 in order of reaction rate. Quenching reactions with O_2 dominate over the inert species present and are therefore the reactions listed for a comparison. Ozone is the most stable with $O_2(a^1\Delta_g)$ also having long lifetime. All other species are quenched many times faster.

Beyond the gas phase kinetics, the wall quenching effects have to be considered. Many species can be transported significant distances with inert wall surfaces. Therefore, by coating all wall surfaces with quartz or using quartz tubes is essential to ensure minimal quenching. Some examples of the relative reaction probabilities of plasma-produced species with a wall surface of Pyrex (similar to quartz) are shown in Table 2. Therefore, having large

Table 1
Reaction rates of plasma-produced oxygen species at 298 K. The term "HP" refers to the high pressure limit.

Reaction	Reaction constant (cm^3/molecule/s)
$O + O_2 + M \rightarrow O_3 + M$	6.0×10^{-34} = (HP limit 3.61×10^{-10}) [40]
$O(^1D) + O_2 \rightarrow O + O_2$	4.0×10^{-11} [40]
$O_2(v) + O_2 \rightarrow O_2 + O_2$	1.73×10^{-13} [41]
$O_2(b^1\Sigma_g) + O_2 \rightarrow O_2 + O_2$	4.1×10^{-17} [40]
$O_2(a^1\Delta_g) + O_2 \rightarrow O_2 + O_2$	1.6×10^{-18} [40]
$O_2(a^1\Delta_g) + Ar \rightarrow O_2 + Ar$	1.0×10^{-20} [42]

Table 2
Wall quenching probabilities of plasma-produced species for a Pyrex surface.

Wall reaction	Reaction probability
$O_2(a^1\Delta_g) + wall \rightarrow O_2$	2×10^{-5} [43]
$O_2(b^1\Sigma_g) + wall \rightarrow O_2$	2×10^{-2} [43]
$O_2(v) + wall \rightarrow O_2$	0.2 [41]
$O(^1D) + wall \rightarrow O(^3P)$	1.0 [43]
$O(^1S) + wall \rightarrow O(^3P)$	1.0 [43]
$O + wall \rightarrow \frac{1}{2}O_2$	2×10^{-2} [43]
$M^+ + wall \rightarrow M$	1.0 [41]

surface to volume ratios in the flow will help to suppress the concentrations of all species except O_3 and $O_2(a^1\Delta_g)$.

There remained the need to isolate O_3 and $O_2(a^1\Delta_g)$ to observe their individual effects. Ozone can be isolated by simply using higher pressures because the $O_2(a^1\Delta_g)$ will be collisionally quenched to $O_2(X^3\Sigma_g)$. This was demonstrated in part I of this two part work [44]. To isolate $O_2(a^1\Delta_g)$, a different approach needs to be taken to remove O_3. To mitigate the effect of O_3 and completely isolate the effect of $O_2(a^1\Delta_g)$, NO was added to the flow downstream of the plasma in the flow diagnostics system, as well as the combustion system. The addition of NO in prescribed concentrations served two purposes. First, it catalytically removed O_3 from the system to isolate $O_2(a^1\Delta_g)$ and second, NO addition in the concentrations in the experiments would not interfere with the effects of $O_2(a^1\Delta_g)$.

The isolation of $O_2(a^1\Delta_g)$ with NO addition relies upon the reaction of NO with O_3 via

$$NO + O_3 \rightarrow NO_2 + O_2 \qquad (2)$$

Reaction (2) is over three orders of magnitude faster than NO with $O_2(a^1\Delta_g)$, as shown in Table 3. Furthermore, the subsequent reaction of NO_2 with $O_2(a^1\Delta_g)$ is also slow in comparison to reaction (2). The major consumption pathway of NO_2 would be from the reaction with O atoms via

$$NO_2 + O \rightarrow NO + O_2 \qquad (3)$$

Since O and O_3 are present at the same location in the flow tube, i.e., O atoms are converted to O_3, NO acts as a catalyst and very little is needed to fully eliminate the O_3. Therefore, the individual effects of $O_2(a^1\Delta_g)$ can be selected by the use of NO addition. Finally, the presence of NO can also be used to determine the presence of O atoms via the well known O atom titration reaction

$$NO + O \rightarrow NO_2^* \rightarrow NO_2 + h\nu \qquad (4)$$
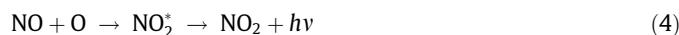
The absence of the greenish-yellow glow in the plasma afterglow is used to assure that all the O atoms are quenched and not present in the flow system.

3. Results and discussion

3.1. NO Addition for $O_2(a^1\Delta_g)$ Isolation

To investigate the flame speed enhancement by $O_2(a^1\Delta_g)$, reduced pressures were used to suppress the quenching and recom-

Table 3
Reaction rates of $O_2(a^1\Delta_g)$ and O_3 with NO and NO_2 at 298 K.

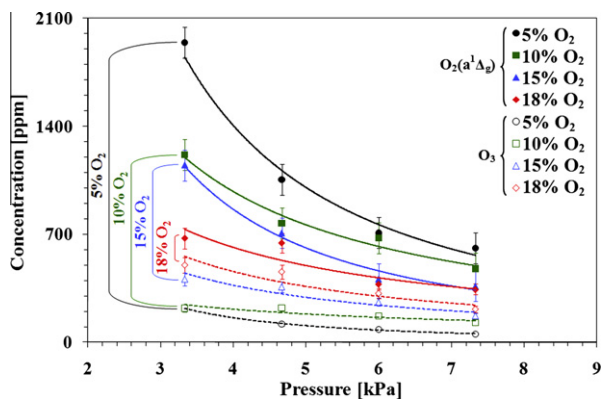| Reaction	Reaction constant (cm^3/molecule/s)
$O_2(a^1\Delta_g) + NO \rightarrow O_2 + NO$	4.48×10^{-17} [45]
$O_2(a^1\Delta_g) + NO \rightarrow O + NO_2$	4.88×10^{-18} [42]
$O_2(a^1\Delta_g) + NO_2 \rightarrow O_2 + NO_2$	5.00×10^{-18} [42]
$O_3 + NO \rightarrow O_2 + NO_2$	1.80×10^{-14} [40]
$O_3 + NO_2 \rightarrow O_2 + O_2 + NO$	1.00×10^{-18} [46]

Fig. 6. Experimentally measured concentrations of O_3 and $O_2(a^1\Delta_g)$ as a function of pressure before O_3 reduction by NO addition.

bination rates. The ICOS and O_3 absorption diagnostics were used to initially measure $O_2(a^1\Delta_g)$ and O_3 as a function of pressure and O_2 concentrations. The results in Fig. 6 show that there remain significant concentrations of O_3, despite the decrease of the pressure. At lower pressure and O_2 loading in Ar, the $O_2(a^1\Delta_g)$ was in significantly greater concentration than O_3. Unfortunately, stable flames under lower pressure and O_2 loadings were difficult to achieve. Therefore, the removal of O_3 was warranted for the isolated study of $O_2(a^1\Delta_g)$.

The results in Fig. 7 show that the addition of NO suppressed the concentration of O_3 to a magnitude below the threshold that could be measured (ppm levels) while the $O_2(a^1\Delta_g)$ concentration at a given residence time increased by almost an order of magnitude over a wide pressure range. Since the NO addition worked catalytically to reduce the $O_2(a^1\Delta_g)$ quenching species of O_3 and O through reactions (2) and (3), the process was heavily reliant upon the concentration of O where the NO was added to the system. With the flow rates used in the system, the residence time between the plasma and the location of NO addition was approximately 5 ms. For the pressures used in the experiments, there was a significant concentration of O in relation to O_3. Nevertheless, the concentrations of NO and NO_2 needed to be verified to ensure that the NO_2 concentration remained negligible.

To confirm that there was no conversion of NO to NO_2, measurements were taken using the FTIR with the plasma off and on. The measurements were taken initially of the plasma off where the FTIR measured the exact concentration of NO that was being added to the system. When the plasma was turned on, the NO concentration did not change, as shown in Fig. 8. To confirm further that
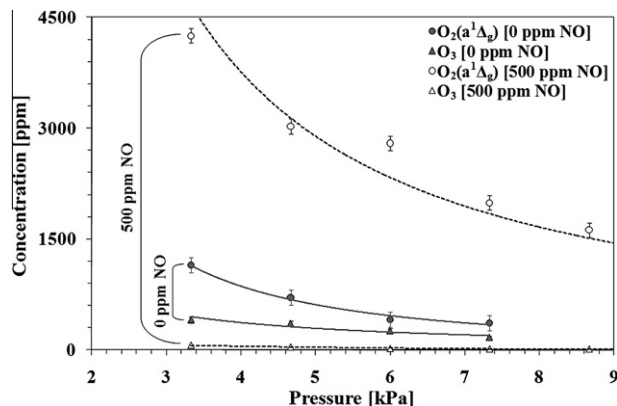

Fig. 7. Experimentally measured concentrations of $O_2(a^1\Delta_g)$ and O_3 with and without 500 ppm NO for 15% O_2 in 85% Ar as a function of pressure.
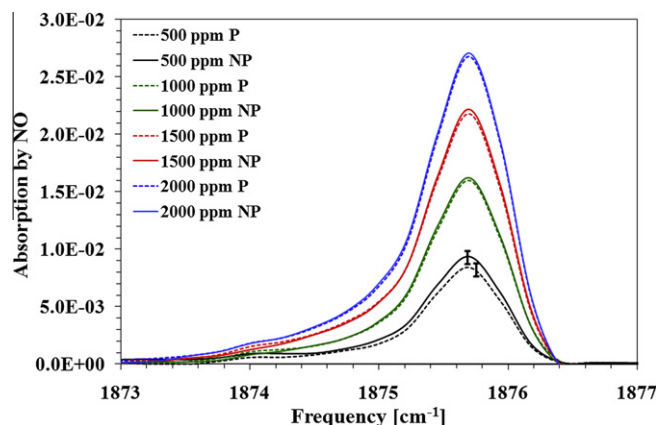

Fig. 8. NO absorption measurements from FTIR showing that the NO concentrations did not change with the plasma on or off and therefore no conversion to NO_2 (P and NP are plasma and no plasma, respectively).
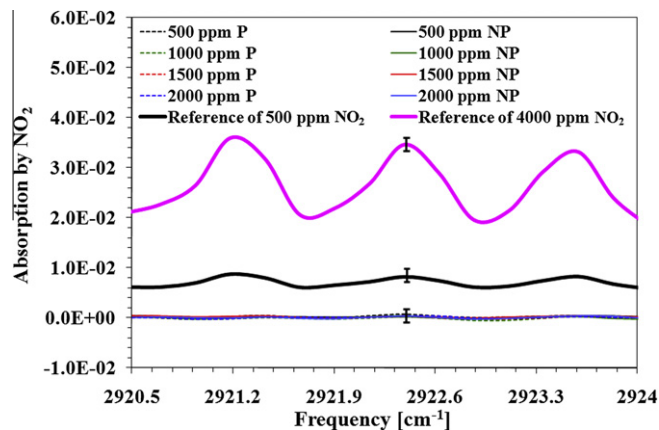

Fig. 9. NO_2 absorption measurements from FTIR showing that the NO is not converted to NO_2 when the plasma is on or off (P and NP are plasma and no plasma, respectively).

there was no NO_2 production, Fig. 9 shows that the concentration of NO_2 remained below the detectability threshold of the FTIR. Two reference absorption spectrums of 500 ppm and 4000 ppm of NO_2 that were taken at the same pressures and temperatures are shown for comparison and that the three peaks present can be resolved. The results show clearly that the highest concentration of NO_2 was on the order of 10's of ppm. Since flame speed enhancement by NO_2 is more than a factor of three smaller than the effect of O_3 for the same concentrations, the small concentration of NO_2 would have a negligible effect on flame speed. Therefore, when NO was added to the plasma afterglow, the only plasma-produced species to survive would be $O_2(a^1\Delta_g)$ and the NO concentration would remain constant.

To confirm further the chemical kinetic processes involved in the post-discharge gases in the system, a simple flow kinetic model was compiled to include O, O_3, $O_2(a^1\Delta_g)$, N_2, NO, NO_2, and Ar. Other excited species were excluded because they existed in only small concentrations at the point of NO injection, which was the starting point for the numerical simulations. Specifically, $O_2(b^1\Sigma_g)$ was excluded because it would be more than an order of magnitude lower in concentration than $O_2(a^1\Delta_g)$ and would also quench rapidly [35]. Nitrogen was included in the model because the NO being injected into the system downstream of the plasma was accompanied by N_2. The presence of N_2 did not affect any of the results because it did not react with any of the other species present in

the system. The most critical reaction would be with $O_2(a^1\Delta_g)$, but the quenching rate is of the same order as the rate with Ar [43]. One of the most important initial conditions for the numerical simulations was the concentration of atomic oxygen. To find what concentrations existed in the experiments, an NO_2 titration technique was adopted [47]. The NO_2 was added to the plasma afterglow at the same location of NO injection, approximately 5 ms downstream of the plasma. The NO_2 titration technique works by reaction (3) being five orders of magnitude faster than reaction (4). Therefore, when NO_2 was injected after the plasma, the FTIR was used to sample the flow downstream and monitor the NO versus NO_2 concentration. The NO_2 was continually added until the FTIR showed the presence of NO_2 and no changes in the concentration of NO. At that point, the concentration of NO_2 being added was equal to the concentration of O at the injection location in the flow. Furthermore, the lack of emission from reaction (4) would also indicate that there was no longer O present in the flow. The NO_2 titration technique provided quantification of the O concentration within a 10% uncertainty to be used as an initial condition in the kinetic model.

Without NO addition to the plasma afterglow, the model predicted the concentrations of O_3 and $O_2(a^1\Delta_g)$ well. With NO addition, it was found that if the simple flow kinetic model was maintained at 300 K, the catalytic cycle to remove O_3 was not complete and produced significant concentrations of NO_2. The results indicated that reaction (3) was not participating, possibly from the lack of presence of O. Realizing that the temperature of the gas in the plasma afterglow is not 300 K, but starts at a temperature around 450 K and decreases to nearly room temperature after a short residence time, the model was adjusted to account for this. With a prescribed temperature gradient, the results with NO addition showed clearly that the catalytic cycle did not consume any NO and the NO_2 remained negligible (Fig. 10). Furthermore, the results without NO addition agreed well with the experiments (Fig. 10). The temperature gradient was critical to the catalytic cycle because of the quenching reactions of atomic oxygen. When the temperature was fixed at 300 K, the O quenched quickly to produce O_3, therefore not allowing the NO_2 to be converted back to NO. When the temperatures were higher at the beginning of the computation, the recombination reactions were suppressed, allowing for the catalytic cycle to complete.

The validation of the simple flow model with the experimental results allowed for it to be used to find the concentrations of $O_2(a^1\Delta_g)$ at the residence time of where the flame was in the burner system. Furthermore, the change of $O_2(a^1\Delta_g)$ concentration at

the residence time of the flame was very small, allowing for minimal error. Therefore, the $O_2(a^1\Delta_g)$ could be measured in the ICOS cavity and the kinetic model used to find the actual concentration at the specific flow residence time where the flame was located in the combustion system.

3.2. Experimental results of flame propagation enhancement by $O_2(a^1\Delta_g)$

To examine the effects of $O_2(a^1\Delta_g)$ on flame propagation speed, C_2H_4 was used as the fuel to produce stable lifted flames at low pressures. The co-flow conditions of velocity and O_2 concentration in Ar were fixed, along with the fuel jet velocity to establish a flame at a stationary lifted location. Photographs were taken of the flame while simultaneously recording the pressure and temperature. The microwave plasma was then turned on and photographs taken again of the flame with a lower liftoff height. The change in flame liftoff height was calculated from the photographs. A similar procedure was used again with NO addition just downstream of the microwave plasma cavity, replicating the residence times in the plasma afterglow diagnostics system. The results showed that there was a significant change in the flame liftoff height when the plasma was turned on with and without the addition of NO. Therefore, the flame propagation enhancement came from a combination of O_3 and $O_2(a^1\Delta_g)$ without NO addition and only from $O_2(a^1\Delta_g)$ with NO addition. Concentrations between 500 ppm and 2000 ppm of NO were added downstream of the plasma to give different concentrations of $O_2(a^1\Delta_g)$ at the flame front. The more NO that was added, the faster the O_3 and O were removed before they reacted with and quenched $O_2(a^1\Delta_g)$.

The experiments were performed for several conditions at both 3.61 kPa and 6.73 kPa. The flow field, temperature, and pressure remained constant when the plasma was cycled off and on, so a direct comparison between plasma off and on can be attributed to the enhancement by O_3 and $O_2(a^1\Delta_g)$. The temperature and pressure remained constant within an uncertainty of 0.1 K and 26.7 Pa respectively. Experiments were performed to quantify that the uncertainty in temperature and pressure was not affecting the flame liftoff height enough to mask the enhancement by O_3 and $O_2(a^1\Delta_g)$ addition. For a temperature change of 0.1 K, the flame liftoff height changed by 0.07 mm and for a pressure change of 26.7 Pa the flame liftoff height changed by 0.29 mm. Therefore, for the change in flame liftoff height observed in the experiments with O_3 and $O_2(a^1\Delta_g)$ addition, which was on the order of 5 mm to 10 mm, the uncertainty was more than an order of magnitude smaller.

Also of significance to note was that the presence of NO did affect the flame structure by changing the stoichiometric contour and flame speed slightly, but the comparison was between the plasma being off and on with constant NO addition. Furthermore, since the flow diagnostics showed that the NO acted catalytically to reduce the O_3 and did not change in concentration, the conditions of the plasma being off and on could be compared directly to each other. The near zero concentrations of NO_2 would have a negligible effect on flame speed since the enhancement was calculated to be more than three times lower than that of O_3.
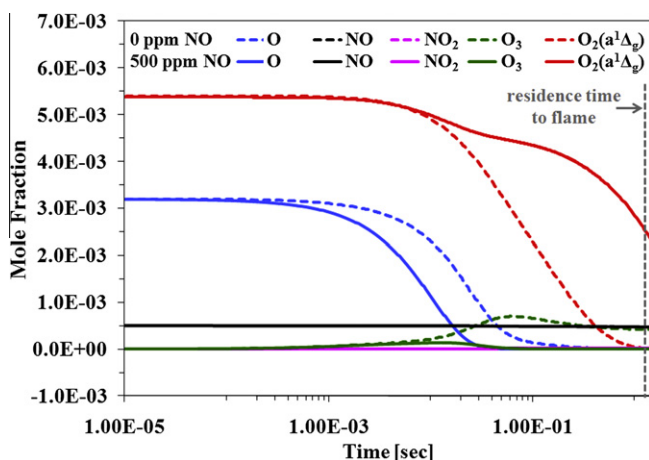

Fig. 10. Plot of numerical simulation results of plasma afterglow species profiles with and without NO addition.

Table 4
Change in flame liftoff height (ΔH_L) with simulation corrected concentrations of $O_2(a^1\Delta_g)$ and O_3 present at flame for a plasma power of 80 W at 3.61 kPa.

$O_2(a^1\Delta_g)$ (ppm)	O_3 (ppm)	ΔH_L (mm)
215	513	7.15
3851	0	4.76
5416	0	7.31
5571	0	6.82
5596	0	6.83

Table 5
Change in flame liftoff height (ΔH_L) with simulation corrected concentrations of $O_2(a^1\Delta_g)$ and O_3 present at flame for a plasma power of 80 W at 6.73 kPa.

$O_2(a^1\Delta_g)$ (ppm)	O_3 (ppm)	ΔH_L (mm)
10	423	7.70
2345	0	1.91
3285	0	5.64
3391	0	6.11

The same O_2 loadings, flow rates, and pressures were then used on the plasma afterglow diagnostics system to find the concentrations of O_3 and $O_2(a^1\Delta_g)$ that were present at the lifted flame. The measured concentrations of O_3 and $O_2(a^1\Delta_g)$ were corrected for residence time using the kinetic model described in Section 3.1. The results are shown in Tables 4 and 5 as a function of O_3 and $O_2(a^1\Delta_g)$ concentration for 3.61 kPa and 6.73 kPa, respectively. Overall with NO addition, there was no change in the flow field, temperature, or any species other than $O_2(a^1\Delta_g)$ when the plasma was cycled on and off. Therefore, by turning on the plasma, it was the equivalent of introducing a pure source of $O_2(a^1\Delta_g)$. The results in Tables 4 and 5 show that there was a clear correlation between the concentration of $O_2(a^1\Delta_g)$ present and the change in flame liftoff height. Fig. 11 shows the trend of increasing change in flame liftoff height, and hence more flame speed enhancement, with increasing $O_2(a^1\Delta_g)$ concentration for both 3.61 kPa and 6.73 kPa. The experimental uncertainties for the change in flame liftoff height was ±0.5 mm and for $O_2(a^1\Delta_g)$ concentration was ±500 ppm, and are shown by the error bars in Fig. 11.

With the results showing clearly the enhancement of flame propagation speed by $O_2(a^1\Delta_g)$, it was important to determine the enhancement quantitatively. Unlike the lifted flame at atmospheric pressure described in the first part of this work related to O_3, a cold flow similarity solution does not correctly describe the low pressure experiments. Therefore, an indirect method was used to find the amount of flame speed enhancement quantitatively. The change in flame liftoff height shown in Tables 4 and 5, and Fig. 11 indicate that approximately ten times the amount of $O_2(a^1\Delta_g)$ (approximately 5500 ppm) was needed to achieve the same enhancement as O_3 (approximately 500 ppm). Since the enhancement of flame propagation speed was established with the addition of O_3 (shown in the part I companion paper) [44], it can be used to quantify the enhancement by $O_2(a^1\Delta_g)$. The C_2H_4 laminar and lifted flame speed enhancement was computed using the C_2H_4 kinetic mechanisms [48,49] with the addition of the O_3 reactions shown in part I of this work [44]. The laminar and lifted
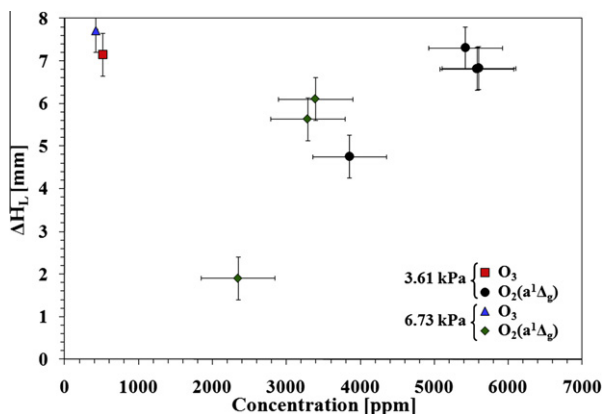

Fig. 11. Plot of experimental results of flame liftoff change with $O_2(a^1\Delta_g)$ and O_3 concentration for a plasma power of 80 W. The error bars denote the experimental uncertainties in the concentrations and change in flame liftoff height.
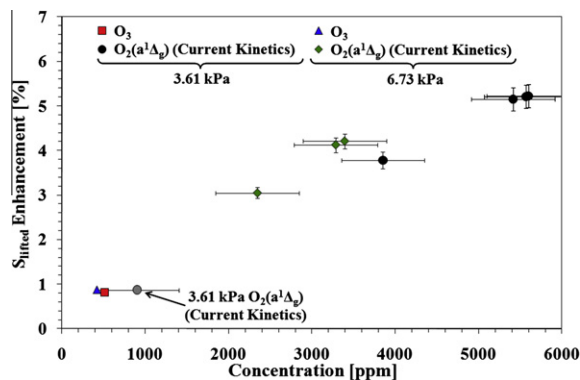

Fig. 12. Plot of computational results of lifted flame speed enhancement with $O_2(a^1\Delta_g)$ and O_3. The horizontal error bars denote the propagation of uncertainty from the concentrations found experimentally, while the vertical error bars denote the range of lifted flame speed enhancement when using the different published reaction rates.

flame speed are related through the square root of the density ratio [44], therefore the percent enhancement of the flame speeds were comparable. Furthermore, all of the experiments were performed for large flame liftoff heights where the mixture fraction gradient is small and there is the closest agreement to the numerical simulations at a zero mixture fraction gradient. Therefore, the lifted flame speed enhancement was used for comparison between experiments and numerical simulations. The results for the conditions of 500 ppm of O_3 addition at 3.61 kPa and 6.73 kPa showed approximately 1% enhancement of the lifted flame speed (Fig. 12). Therefore, since the flame liftoff height change for 500 ppm O_3 is equivalent to 5500 ppm $O_2(a^1\Delta_g)$, it was reasonable to assume that their effects on flame speed enhancement were comparable. The overall lifted flame speed enhancement would be higher because of the kinetic-induced hydrodynamic enhancement described in part I of this work [44]. If the effect of O_3 at low pressure is comparable to what was found at high pressure, then 5500 ppm of $O_2(a^1\Delta_g)$ will give approximately 2–3% enhancement of the lifted flame speed.

3.3. Computational analysis with current kinetics of $O_2(a^1\Delta_g)$

Numerical simulations were performed in order to explain the enhancement mechanism with the addition of $O_2(a^1\Delta_g)$. The C_2H_4 combustion mechanisms [48,49] with the O_3 reactions added [44] were used along with the inclusion of $O_2(a^1\Delta_g)$ reactions. The reactive and collisional quenching rates of $O_2(a^1\Delta_g)$ with oxygen and inert species as a function of temperature have been well studied and were used to compute the cold flow transport of $O_2(a^1\Delta_g)$ in the ICOS system and prior to the flame in the combustion system, as shown in Section 3.1. These $O_2(a^1\Delta_g)$ reactions were added to the C_2H_4/O_3 mechanisms. The reactions of $O_2(a^1\Delta_g)$ with the fuel have also been well studied at 298 K, but there is little data at intermediate and high temperatures. The most studied $O_2(a^1\Delta_g)$ reactions applicable to a combustion system are for H_2–O_2 mixtures. These reactions of hydrogen and oxygen containing species with $O_2(a^1\Delta_g)$ are shown in Table 6 and have been compiled specifically for H_2–O_2 mixtures activated by plasma. The rates were taken from previous numerical work on plasma-assisted H_2–O_2 combustion systems, as well as from specific reaction rate studies [27,29,50–53]. There are a few differences that arose, specifically regarding the two reactions

$$H + O_2(a^1\Delta_g) \rightarrow O + OH \qquad (5)$$

$$H_2 + O_2(a^1\Delta_g) \rightarrow H_2 + O_2 \qquad (6)$$

Table 6
Reaction rates of $O_2(a^1\Delta_g)$ with hydrogen containing species.

Reaction	Reaction constant (cm^3/molecule/s)	Temperature dependence	Activation energy (kJ/mole)
Reactive quenching of $O_2(a^1\Delta_g)$			
$H + O_2 \rightarrow O + OH$ [50]	5.00×10^{-9}	0	60.3
$H + O_2(a^1\Delta_g) \rightarrow O + OH$ [51]	1.82×10^{-10}	0	26.5
$H + O_2(a^1\Delta_g) \rightarrow O + OH$ [29]	6.55×10^{-11}	0	21.0
$OH + O_2(a^1\Delta_g) \rightarrow O + HO_2$ [51]	2.16×10^{-11}	0	141.4
$OH + O_2(a^1\Delta_g) \rightarrow H + O_3$ [51]	7.31×10^{-17}	1.44	226.4
$H_2 + O_2(a^1\Delta_g) \rightarrow OH + OH$ [51]	2.82×10^{-9}	0	141.4
$H_2 + O_2(a^1\Delta_g) \rightarrow HO_2 + H$ [51]	4.13×10^{-12}	0	151.6
$H_2O + O_2(a^1\Delta_g) \rightarrow OH + HO_2$ [27]	9.03×10^{-8}	0.5	209.7
$H_2O + O_2(a^1\Delta_g) \rightarrow O + H_2O_2$ [27]	2.05×10^{-12}	0.5	283.5
Collisional quenching of $O_2(a^1\Delta_g)$			
$H_2 + O_2(a^1\Delta_g) \rightarrow H_2 + O_2$ [52]	2.16×10^{-13}	0	21.6
$H_2 + O_2(a^1\Delta_g) \rightarrow H_2 + O_2$ [29]	1.68×10^{-12}	0	32.0
$H + O_2(a^1\Delta_g) \rightarrow H + O_2$ [51]	6.97×10^{-16}	0	0
$OH + O_2(a^1\Delta_g) \rightarrow OH + O_2$ [51]	5.65×10^{-18}	0	0
$HO_2 + O_2(a^1\Delta_g) \rightarrow HO_2 + O_2$ [51]	5.65×10^{-18}	0	0
$H_2O + O_2(a^1\Delta_g) \rightarrow H_2O + O_2$ [51]	5.65×10^{-18}	0	0
$H_2O_2 + O_2(a^1\Delta_g) \rightarrow H_2O_2 + O_2$ [51]	5.65×10^{-18}	0	0
Other reactions with $O_2(a^1\Delta_g)$			
$H + HO_2 \rightarrow H_2 + O_2(a^1\Delta_g)$ [51]	3.32×10^{-12}	0	2.4
$OH + O \rightarrow H + O_2(a^1\Delta_g)$ [51]	9.63×10^{-12}	0	51.8
$O_3 + OH \rightarrow HO_2 + O_2(a^1\Delta_g)$ [51]	7.97×10^{-13}	0	8.3
$O_3 + HO_2 \rightarrow OH + O_2 + O_2(a^1\Delta_g)$ [51]	1.66×10^{-14}	0	8.3
$HO_2 + HO_2 \rightarrow H_2O_2 + O_2(a^1\Delta_g)$ [51]	1.49×10^{-11}	0	4.2
$H_2O_2 + O \rightarrow H_2O + O_2(a^1\Delta_g)$ [51]	6.97×10^{-13}	0	17.7

There was a small difference in reaction (5) between Refs. [29] and [51], as well as in reaction (6) between Refs. [29] and [52], as shown in Table 6. The differences in the reported reaction rates will be discussed in relation to the sensitivity of the computed flame speed enhancement shortly.

The reactions were added to the C_2H_4/O_3 kinetic mechanisms and the results are shown in Fig. 12 using the concentrations of O_3 and $O_2(a^1\Delta_g)$ from the experiments. The results of enhancement using the $O_2(a^1\Delta_g)$ concentrations found in the experiments showed flame speed enhancement of more than 5%. When compared to the results of lifted flame speed enhancement by O_3 (which was found to be approximately 1%) there was a large discrepancy compared with the experimental results, which was well outside the uncertainties for the system. For example, in the experiments at 3.61 kPa, the change in flame liftoff height for 500 ppm O_3 was approximately equal to 5500 ppm $O_2(a^1\Delta_g)$ (Fig. 11). According to the numerical simulations, there was more than a factor of five difference in the enhancement of flame speed. Considering that the O_3 and $O_2(a^1\Delta_g)$ should both enhance the lifted flame speed similarly with the lean and rich enhancement more than stoichiometric [31,32], there is a significant error in the $O_2(a^1\Delta_g)$ kinetic calculations. With regard to the differences in the rates for reactions (5) and (6), the deviations in the flame speed enhancement was no more than ±4%. The vertical error bars in Fig. 12 show the negligible enhancement differences when using the two published rates for reactions (5) and (6) and therefore the sensitivity of the flame speed to the differences in reaction rates do not account for the significant deviations from the experiments.

To understand what caused the significant flame speed enhancement by $O_2(a^1\Delta_g)$, a rate of production plot of $O_2(a^1\Delta_g)$ in the flame is shown in Fig. 13. The major consumption pathways of $O_2(a^1\Delta_g)$ was from the branching reaction with H, with some contribution of collisional quenching by H_2. The reaction of $O_2(a^1\Delta_g)$ with H will significantly enhance the flame since it is a primary radical branching reaction. Therefore, it was reasonable that the enhancement was so large in the numerical simulations.

The changes in the radical pool in the earlier stages of the flame were plotted and are shown in Fig. 14. In the earlier stages of the
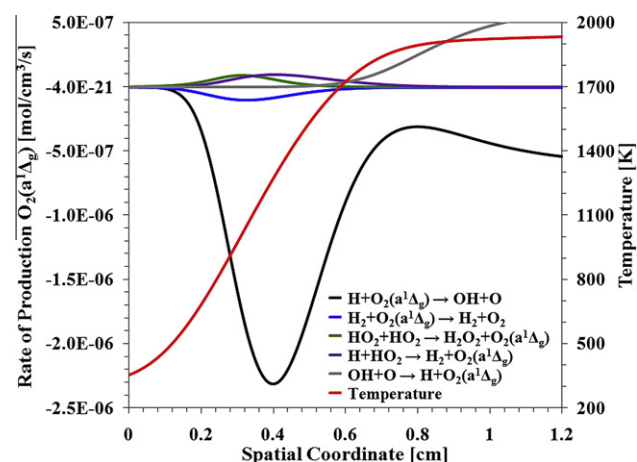

Fig. 13. Rate of production plot of $O_2(a^1\Delta_g)$ superimposed on the temperature profile showing the major consumption pathways of $O_2(a^1\Delta_g)$ with current published rate data with hydrogen containing species.

flame where the temperature is slightly elevated between 400 K and 500 K, the $O_2(a^1\Delta_g)$ begins to be consumed, causing a decrease in the C_2H_4 concentration and a subsequent increase in O and OH. The increase in concentration of OH would provide chemical heat release through subsequent reactions earlier in the flame to enhance the overall flame speed significantly. These results of higher concentrations of OH in the earlier stages of the flame leading to chemical heat release and enhanced flame speed was shown in part I of this work through the study of O_3 addition [44]. The increase in the radical pool concentration of O from the reactions with $O_2(a^1\Delta_g)$ were investigated in more depth through a rate of production analysis. The results showed that the major pathway for O consumption was from the reaction with the parent fuel, C_2H_4, and its fragment, CH_3. The end results of flame propagation enhancement came from the increased radical pool concentration and extraction of chemical heat release earlier in the flame compared to the results with no $O_2(a^1\Delta_g)$ addition. Fig. 15 clearly indi-
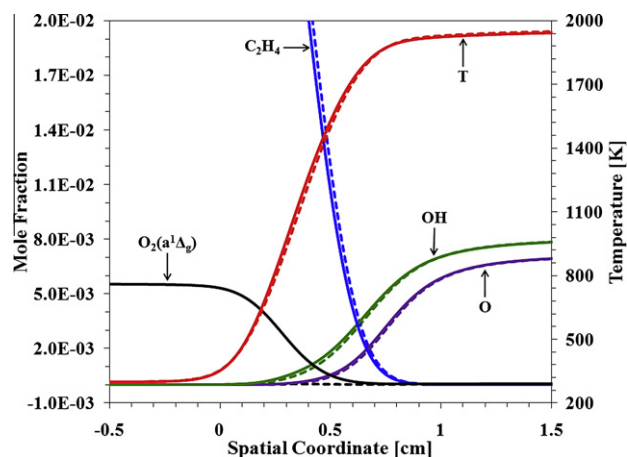
Fig. 14. Temperature and mole fraction profiles, dashed lines = w/o $O_2(a^1\Delta_g)$, solid lines = w/$O_2(a^1\Delta_g)$.
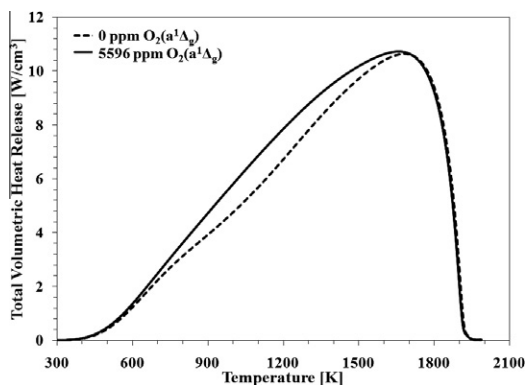

Fig. 15. Heat release versus temperature showing elevated levels of chemical heat release at lower temperatures with $O_2(a^1\Delta_g)$ addition.

cates the elevated levels of chemical heat release result by showing the total volumetric heat release as a function of temperature in the flame. There is significantly more heat release between 800 K and 1500 K with $O_2(a^1\Delta_g)$ addition, which aligns well with the peak consumption of $O_2(a^1\Delta_g)$ and elevated radical concentrations shown in Figs. 13 and 14, respectively.

3.4. Inclusion of $O_2(a^1\Delta_g)$ quenching by hydrocarbons

With an understanding of how $O_2(a^1\Delta_g)$ enhanced the flame speed in the numerical simulations, it becomes apparent that there are two possible explanations for the discrepancy shown in Fig. 12 with respect to the enhancement by O_3 and $O_2(a^1\Delta_g)$. First, a significant concentration of the $O_2(a^1\Delta_g)$ could quench before reacting with H. The collisional quenching reactions of $O_2(a^1\Delta_g)$ with the parent fuel or its fuel fragments could decrease the concentration significantly, therefore leading to less enhancement. To achieve the same enhancement wih $O_2(a^1\Delta_g)$ as the calculations with O_3, there would need to be approximately 900 ppm $O_2(a^1\Delta_g)$ (shown in Fig. 12 for 3.61 kPa). Therefore, approximately 4600 ppm of $O_2(a^1\Delta_g)$ would have to collisionally quench, allowing only a small fraction of the original concentration to react with H. The enhancement would be less, especially if the dominating reactions of $O_2(a^1\Delta_g)$ are with the parent fuel and not providing chain branching as in the reaction of H with $O_2(a^1\Delta_g)$. Second, there could be a combination of reactive and collisional quenching pathways for

Table 7
Reaction rates of $O_2(a^1\Delta_g)$ with hydrocarbon species. (*low) = estimated rate with low activation energy, (*high) = estimated rate with high activation energy, (*exp. fit) = estimated rate with activation energy to fit trend of experimental results, (*) = estimated rate.

Reaction	Reaction constant (cm^3/molecule/s)	Temperature dependence	Activation energy (kJ)
$CH_4 + O_2(a^1\Delta_g) \rightarrow CH_4 + O_2$ [42]	1.40×10^{-18}	0	0
$CH_4 + O_2(a^1\Delta_g) \rightarrow CH_3 + HO_2$ [54]	6.14×10^{-12}	0	149.0
$C_2H_4 + O_2(a^1\Delta_g) \rightarrow C_2H_4 + O_2$ (*low)	7.71×10^{-16}	0	15.0
$C_2H_4 + O_2(a^1\Delta_g) \rightarrow C_2H_4 + O_2$ (*high)	3.12×10^{-13}	0	30.0
$C_2H_4 + O_2(a^1\Delta_g) \rightarrow C_2H_4 + O_2$ (*exp. fit)	5.46×10^{-10}	0	48.6
$C_2H_4 + O_2(a^1\Delta_g) \rightarrow C_2H_3 + HO_2$ (*)	7.01×10^{-11}	0	146.5

$O_2(a^1\Delta_g)$ that could be responsible for the enhancement observed in the experiments.

The reactive and collisional quenching rates for some of the hydrocarbon species were added to the kinetic mechanism one at a time to test the sensitivity of flame speed enhancement. In Table 7 is a list of the reactions along with their rates. Initially the reactions with CH_4 of

$$CH_4 + O_2(a^1\Delta_g) \rightarrow CH_4 + O_2 \tag{7}$$

$$CH_4 + O_2(a^1\Delta_g) \rightarrow CH_3 + HO_2 \tag{8}$$

were added, but did not change the flame speed enhancement, which was reasonable considering the low concentrations of CH_4 in the system. Next, noting that the inclusion of $O_2(a^1\Delta_g)$ collisional quenching by the parent fuel H_2 in an H_2–O_2 system via reaction (6) was found in previous numerical investigations to be significant and decreased the effectiveness of $O_2(a^1\Delta_g)$ enhancement [29], it is reasonable to include collisional quenching by the parent fuel via

$$C_2H_4 + O_2(a^1\Delta_g) \rightarrow C_2H_4 + O_2 \tag{9}$$

for our hydrocarbon fueled combustion system. There are some collisional quenching rates for $O_2(a^1\Delta_g)$ with C_2H_4 and other small hydrocarbon fuels, but they are only at 298 K [42,52]. To the authors knowledge, there are no verified quenching rates of hydrocarbon species (specifically C_2H_4) with $O_2(a^1\Delta_g)$ in the intermediate to high temperature range where they would be the most important for a flame system.

The work of Borrell and Richards found that the temperature dependence of $O_2(a^1\Delta_g)$ quenching by H_2 was approximately Arrhenius [53], and that other species also follow an Arrhenius
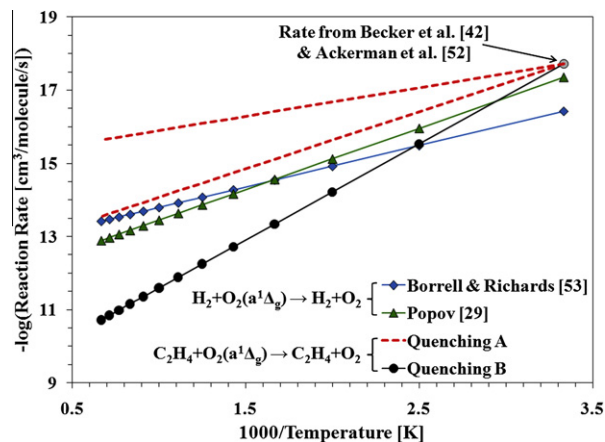

Fig. 16. Arrhenius temperature dependent collisional quenching rates of $O_2(a^1\Delta_g)$ by H_2 and C_2H_4. The rates with C_2H_4 are estimates.

temperature dependence. Therefore, it was assumed that C_2H_4 might also follow this temperature dependence for quenching $O_2(a^1\Delta_g)$. Originating with the quenching rate of $O_2(a^1\Delta_g)$ by C_2H_4 at 298 K [42,52], an Arrhenius temperature dependent rate was estimated to explain the trend discrepancy shown in the experimental results of Fig. 12. Three different temperature dependencies were chosen with a range of activation energies. Previously published temperature dependent collisional quenching rates of $O_2(a^1\Delta_g)$ have shown that the activation energy range is typically between 15 kJ/mole and 20 kJ/mole [55]. Furthermore, the activation energy for the collisional quenching of $O_2(a^1\Delta_g)$ by H_2 is as high as 32 kJ/mole [29]. Therefore, the range of 15–30 kJ/mole was chosen for the activation energies of reaction (9), with a reaction constant chosen in order to agree with published rates at 298 K [42,52]. The envelope of reaction rates for (9) using activation energies from 15 kJ/mole to 30 kJ/mole is shown in Fig. 16 and is labeled as "Quenching A".

Computations were performed using the rates within the envelope of "Quenching A" in Fig. 16 and the results are shown in Fig. 17. The flame speed enhancement decreased slightly, but not enough to explain the discrepancy. In an attempt to explain the disagreement, a rate for reaction (9) was chosen in order to bring the enhancement by $O_2(a^1\Delta_g)$ down to the enhancement by O_3. To accomplish this, a reaction constant of 5.46×10^{-10} cm³/molecule/s and an activation energy of 48.6 kJ/mole were chosen with the temperature dependence shown in Fig. 16 as "Quenching B." By using the "Quenching B" rate for reaction (9), the results of enhancement by O_3 and $O_2(a^1\Delta_g)$ were approximately equal, therefore agreeing with the trends of the experimental results (Fig. 17). A rate of production analysis of $O_2(a^1\Delta_g)$ was performed with the "Quenching B" rate and the major consumption pathway shifted to reaction (9) with negligible consumption by reaction (5). Additionally, the concentration profile of $O_2(a^1\Delta_g)$ showed a more rapid decrease in the earlier stages of the flame, but no appreciable increase in C_2H_4 consumption or O and OH production. Furthermore, the quenching pathway involves electronic-to-vibrational-translational energy transfer [56] which releases so little energy that the translational temperature changed negligibly. The computed temperature profiles confirmed the negligible increase in temperature, and therefore that a significant concentration of $O_2(a^1\Delta_g)$ was consumed and did not affect the flame in the process. The high activation energy and hence strong temperature dependence of reaction (9) given by the estimated rate "Quenching B"

mitigated the computed enhancement discrepancy, but the rate appears unreasonably high and has not been validated and therefore requires further investigations.

Therefore, the last possible explanation of the trend discrepancy in computed enhancement lies in the reactive quenching of $O_2(a^1\Delta_g)$ by C_2H_4 and its fragments. The first assumption was to decrease the activation energy of the reaction

$$C_2H_4 + O_2(a^1\Delta_g) \rightarrow C_2H_3 + HO_2 \qquad (10)$$
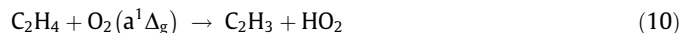
by the energy contained within $O_2(a^1\Delta_g)$. This equates to decreasing the activation energy by 0.98 eV (94.5 kJ/mole), and the rate is shown in Table 7. The inclusion of this reaction in the kinetic mechanism did not result in any change in flame speed enhancement because the rate is slow in comparison to other reaction pathways with C_2H_4 and $O_2(a^1\Delta_g)$. Beyond reaction (10) there could be other possible product pathways which have been investigated through quantum calculations with C_2H_4 [57,58]. The pathways show that $O_2(a^1\Delta_g)$ can attack the double carbon bond to split the parent fuel molecule, possibly providing significant enhancement of fuel oxidation rates by producing CH_2O and other hydrocarbon fragments, but the rates are not known.

Therefore, the results suggest that the probable reactive scheme has both collision and reactive quenching of $O_2(a^1\Delta_g)$ by the parent fuel and its fragments. There remain many unknowns as to the kinetic mechanisms for $O_2(a^1\Delta_g)$ with hydrocarbons under flame conditions. The lack of rate data for these reactions in the intermediate to high temperature range which is applicable to combustion systems remains a significant obstacle and requires further investigation. Nevertheless, the results from this investigation have provided the first experimental data set of flame propagation enhancement by $O_2(a^1\Delta_g)$ which provides a foundation for future investigations.

4. Conclusions

The present study provides a promising approach to isolate and transport plasma-produced excited species for the kinetic study of plasma-assisted combustion. By separating the plasma and combustion system, specific plasma-produced species can be isolated and measured while minimizing the complications of other plasma–flame interactions. Isolation of the specific effects of individual plasma-produced species will have a significant impact on the development of detailed plasma–flame kinetic mechanisms. Through the current work a platform to study quantitatively the enhancement effects of plasma-produced $O_2(a^1\Delta_g)$ on C_2H_4 lifted flame propagation speeds was developed. It was found quantitatively, for the first time, that $O_2(a^1\Delta_g)$ enhances flame propagation. The addition of NO to the plasma afterglow allowed for an order of magnitude increase in the $O_2(a^1\Delta_g)$ concentration at a given residence time by removing the quenching species of O_3 and O. The NO was extremely effective because of the catalytic cycle to remove O_3 and O, as well as having a negligible effect on flame speed. The $O_2(a^1\Delta_g)$ was produced in concentrations of over 5000 ppm to enhance flame propagation of C_2H_4 lifted flames by several percent at 3.61 kPa and 6.73 kPa.

Numerical simulations using currently published collisional and reactive quenching reactions have shown that there is a significant discrepancy in the predicted enhancement compared with the trends found in the experiments. The pathways of enhancement found in the simulations showed that the branching reaction of $O_2(a^1\Delta_g)$ with H provided O and OH early in the reaction zone and increased chemical heat release and flame propagation enhancement. The lack of temperature dependent quenching rate data of $O_2(a^1\Delta_g)$ by hydrocarbon species was suspected to be the main cause for the discrepancy. Estimations of the temperature
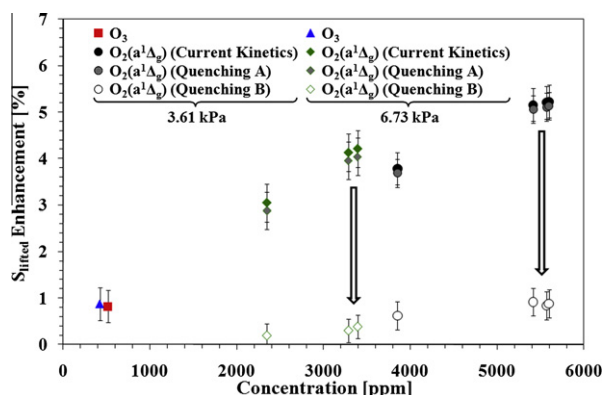
Fig. 17. Plot of computational results of lifted flame speed enhancement with $O_2(a^1\Delta_g)$ and O_3 using the estimated collisional quenching rate of C_2H_4 with $O_2(a^1\Delta_g)$ from Fig. 14. "Quenching A" = inclusion of temperature dependent quenching of $O_2(a^1\Delta_g)$ by C_2H_4 with E_a = 30 kJ/mol, "Quenching B" = inclusion of temperature dependent quenching of $O_2(a^1\Delta_g)$ by C_2H_4 to fit trend of experimental results. The error bars denote the variation in lifted flame speed enhancement when using different C_2H_4 kinetic mechanisms.

dependent collisional quenching rate of $O_2(a^1\Delta_g)$ by C_2H_4 has shown good agreement with the experimental results trends, but the suggested rate appears to be unreasonably high and needs to be validated in future studies. Furthermore, the reactive quenching pathways and their rates remain unknown. Therefore, a combination of both the collisional and reactive quenching rates of $O_2(a^1\Delta_g)$ with hydrocarbon species, specifically the parent fuel molecule, are required in order to correctly explain combustion enhancement. The experimental results have therefore provided the first data of the isolated effect of $O_2(a^1\Delta_g)$ under flame conditions, which is of paramount importance for the development of reaction pathways and plasma–flame kinetic mechanisms. Future investigations are being targeted at establishing temperature dependent quenching rates of $O_2(a^1\Delta_g)$ to enable more accurate and predictive modeling of the plasma–flame interaction.

The experimental results also imply that when energy is coupled into specific plasma-produced species, there is no requirement for the control of heat loss. If energy is coupled into a reactive flow to raise the translational gas temperature only, there needs to be careful thermal management. Whereas, when energy is coupled into energy modes of specific species, no thermal management needs to be considered. The energy contained within the species can be transported for significant distances and residence times and extracted at the combustion reaction zone. Of interest to note is that the plasma power remained constant at 80 W for all conditions with O_3 and/or $O_2(a^1\Delta_g)$ in the current experiments. Therefore, the energy coupled into the flow by the plasma was recovered at the flame. More $O_2(a^1\Delta_g)$ was produced than O_3 for the same plasma power because of the difference in energy to produce these species.

Lastly, in and immediately downstream of an oxygen plasma there would be both O and $O_2(a^1\Delta_g)$, but no O_3 since it is the product of a time-dependent recombination of O and O_2. The O atoms will most likely be more reactive, but there will be higher concentrations of $O_2(a^1\Delta_g)$. Therefore, if oxygen plasma is located closer to a combustion reaction zone, the effects of $O_2(a^1\Delta_g)$ can become more pronounced.

Acknowledgments

References

[1] E. Barbi, J. Mahan, W. O'Brien, T. Wagner, J. Propul. Power 5 (2) (1989) 129–133.
[2] I. Kimura, H. Aoki, M. Kato, Combust. Flame 42 (1981) 297–305.
[3] K. Takita, A. Moriwaki, T. Kitagawa, G. Masuya, Combust. Flame 132 (4) (2003) 679–689.
[4] T. Wagner, W. O'Brien, G.E. Northam, J. Propul. Power 5 (5) (1989) 548–554.
[5] T. Ombrello, Y. Ju, IEEE Trans. Plasma Sci. 36 (6) (2008) 2924–2932.
[6] T. Ombrello, Y. Ju, A. Fridman, AIAA J. 46 (10) (2008) 2424–2433.
[7] T. Ombrello, X. Qin, Y. Ju, A. Gutsol, A. Fridman, AIAA J. 44 (1) (2006) 142–150.
[8] S. Bozhenkov, S. Starikovskaia, A.Y. Starikovskii, Combust. Flame 133 (2003) 133–146.
[9] A. Starikovskii, Proc. Combust. Inst. 30 (2005) 2405–2417.
[10] G. Lou, A. Bao, M. Nishihara, S. Keshav, Y. Utkin, J. Rich, W. Lempert, I. Adamovich, Proc. Combust. Inst. 31 (2007) 3327–3334.
[11] S. Pancheshnyi, D. Lacoste, A. Bourbon, C. Laux, IEEE Trans. Plasma Sci. 34 (6) (2006) 2478–2487.
[12] H. Jagers, A. Von Engel, Combust. Flame 16 (1971) 275–285.
[13] S. Won, M. Cha, C. Park, S. Chung, Proc. Combust. Inst. 31 (2007) 963–970.
[14] S. Won, S. Ryu, M. Kim, M. Cha, S. Chung, Combust. Flame 152 (2008) 496–506.
[15] I. Esakov, L. Grachev, K. Khodatev, V. Vinogradov, D. Van Wie, in: 44th AIAA Aerospace Sciences Meeting and Exhibit, 2006 (AIAA-2006-1212).
[16] Y. Ju, S. Macheret, R. Miles, D. Sullivan, in: 40th AIAA/ASME/SAE/ASEE Joint Propulsion Conference and Exhibit, 2004 (AIAA-2004-2721).
[17] S. Zaidi, S. Macheret, L. Vasilyak, R. Miles, Y. Ju, D. Sullivan, in: 35th AIAA Plasmadynamics and Lasers Conference, 2004 (AIAA-2004-3707).
[18] E. Stockman, S. Zaidi, R. Miles, C. Carter, M. Ryan, Combust. Flame 156 (2009) 1453–1461.
[19] C. Cathey, J. Cain, H. Wang, M. Gunderson, C. Carter, M. Ryan, Combust. Flame 154 (2008) 715–727.
[20] I. Kosarev, N. Aleksandrov, S. Kindysheva, S. Starikovskaia, A. Starikovskii, J. Propul. Power 24 (6) (2008) 1182–1197.
[21] S. Starikovskaia, J. Phys. D: Appl. Phys. 39 (2006) R265–R299.
[22] M. Uddi, N. Jiang, E. Mintusov, I. Adamovich, W. Lempert, Proc. Combust. Inst. 32 (2009) 929–936.
[23] J. Prager, U. Reidel, J. Warnatz. Proc. Combust. Inst. 31 (2007) 1129–1137.
[24] A. Starik, N. Titova, Combust. Expl. Shock Waves 38 (2) (2002) 253–268.
[25] S. Williams, W. Knighton, A. Midley, A. Viggiano, S. Irle, Q. Wang, K. Morokuma, J. Phys. Chem. A 108 (2004) 1980–1989.
[26] A.A. Ionin, I.V. Kochetov, A.P. Napartovich, N.N. Yuryshev, J. Phys. D: Appl. Phys. 40 (2007) R25–R61.
[27] A. Starik, N. Titova, Kinet. Catal. 44 (1) (2003) 28–39.
[28] A. Starik, N. Titova, L. Bezgin, V. Kopchenov, V. Naumov, Czech. J. Phys. 56 (2006) B1357–B1363.
[29] N. Popov, High Temp. 45 (2) (2007) 261–279.
[30] A. Starik, P. Kuleshov, N. Titova, Tech. Phys. 53 (2) (2008) 235–243.
[31] V. Kozlov, A. Starik, N. Titova, Combust. Expl. Shock Waves 44 (4) (2008) 371–379.
[32] A. Bourig, D. Thevenin, J. Martin, G. Janiga, K. Zahringer, Proc. Combust. Inst. 32 (2009) 3171–3179.
[33] G. Smekhov, L. Ibraguimova, S. Karkach, O. Skrebkov, O. Shatalov, High Temp. 45 (3) (2007) 395–407.
[34] O. Skrebkov, S. Karkach, Kinet. Catal. 48 (3) (2007) 367–375.
[35] V. Smirnov, O. Stelmakh, V. Fabelinsky, D. Kozlov, A. Starik, N. Titova, J. Phys. D: Appl. Phys. 41 (19) (2008).
[36] A. Starik, B. Lukhovitskii, V. Naumov, N. Titova, Tech. Phys. 52 (2007) 1281–1290.
[37] A. Starik, N. Titova, Dokl. Phys. 46 (2001) 627–632.
[38] S. Williams, M. Gupta, T. Owano, D. Baer, A. O'Keefe, D. Yarkony, S. Matsika, Opt. Lett. 29 (10) (2004) 1066–1068.
[39] J. Malicet, D. Daumont, J. Charbonnier, C. Parisse, A. Chakir, J. Brion, J. Atmos. Chem. 21 (3) (1995) 263–273.
[40] R. Atkinson, D.L. Baulch, R.A. Cox, J.N. Crowley, R.F. Hampson, R.G. Hynes, M.E. Jenkin, M.J. Rossi, J. Troe, Atmos. Chem. Phys. 4 (2004) 1461–1738.
[41] D.S. Stafford, M.J. Kushner, J. Appl. Phys. 96 (2004) 2451–2465.
[42] K.H. Becker, W. Groth, U. Schurath, Chem. Phys. Lett. 8 (1971) 259–262.
[43] B.F. Gordiets, C.M. Ferreira, V.L. Guerra, J. Loureiro, J. Nahorny, D. Pagnon, M. Touzeau, M. Vialle, IEEE Trans. Plasma Sci. 23 (1995) 750–768.
[44] T. Ombrello, S. Won, Y. Ju, S. Williams, Combust. Flame 157 (10) (2010) 1906–1915.
[45] D.J. Giachardi, G.W. Harris, R.P. Wayne, J. Chem. Soc., Faraday Trans. 2 72 (1976) 619–630.
[46] J. Hjorth, J. Notholt, G. Restelli, Int. J. Chem. Kinet. 24 (1992) 51–65.
[47] A. Ershov, J. Borysow, Plasma Sources Sci. Technol. 16 (2007) 798–802.
[48] H. Wang, A. Laskin, Internal Report, 1998.
[49] H. Wang, X. You, A.V. Joshi, S.G. Davis, A. Laskin, F. Egolfopoulos, C.K. Law, USC Mech. Version II. High-temperature Combustion Reaction Model of $H_2/CO/C_1$–C_4 Compounds, May 2007. <http://ignis.usc.edu/USC_Mech_II.htm>.
[50] NIST Chemical Kinetics Database on the Web, Standard Reference Database 17, Version 7.0 (Web Version), Release 1.4.2, <http://www.kinetics.nist.gov/kinetics/> (accessed 28.11.08).
[51] L. Ibraguimova, G. Smekhov, O. Shatalov, Recommended Rate Constants of Chemical Reactions in an H_2–O_2 Gas Mixture with Electronically Excited Species $O_2(^1\Delta)$, $O(^1D)$, $OH(^2\Sigma)$ Involved, Institute of Mechanics of Lomonosov, Moscow State University, 2003.
[52] R.A. Ackerman, J.N. Pitts, R.P. Steer, J. Chem. Phys. 52 (1970) 1603–1604.
[53] P. Borrell, D.S. Richards, J. Chem. Soc., Faraday Trans. 2 85 (9) (1989) 1401–1411.
[54] S.W. Mayer, L. Schieler, J. Phys. Chem. 72 (1968) 2628–2631.
[55] P. Borrell, P.M. Borrell, D.S. Richards, R.B. Boodaghians, J. Photochem. 25 (1984) 399–407.
[56] J. Plötz, M. Maier, Chem. Phys. Lett. 138 (5) (1987) 419–424.
[57] M. Hotokka, B. Roos, P. Siegbahn, J. Am. Chem. Soc. 105 (16) (1983) 5263–5269.
[58] Y. Yoshioka, T. Tsunesada, K. Yamaguchi, I. Saito, Int. J. Quantum Chem. 65 (1997) 787–801.